Supporting Information

Highly Efficient Solution-Processed Thermally Activated Delayed Fluorescence Emitter Base on Fused Difluoroboron Ketoiminate Acceptor: C/N Switch to Realize Effective Modulation of Luminescence Behavior

Xin Wang[ab], Hua Li[a], Xiaofu Wu[a], Haiyang Shu[ab], Hongkun Tian[ab], Hui Tong*[ab], Lixiang Wang*[ab]

1. Experimental Details

1.1. Materials and Reagents. 4-bromobenzaldehyde, methyl 4-bromobenzoate, 2-methylpyridine, pyridin-2-amine, 9,9-dimethyl-9,10-dihydroacridine (DMAC) and boron trifluoride diethyl etherate ($BF_3 \cdot OEt_2$) were purchased from energy chemical. All solvents were purified and distilled using standard procedures before use. All others were analytical reagents and were used without further purification.

1.2. Physical Measurements and Instrumentation. ^1H NMR, ^{13}C NMR and $^{19}F\{1H\}$ NMR spectroscopy were recorded at 400 MHz (Bruker AV) with TMS as the internal standard. All chemical shifts are given in ppm and all coupling constants (J values) are reported in Hertz (Hz). High-resolution mass spectra were obtained by using LTQ Orbitrap Velos Pro. Thermal analyses were performed on TA-TGA55 under nitrogen atmosphere at a heating rate of 10 ^{o}C/min, in which the decomposition temperature (T_d) is defined as the temperature at which the material showed a 5% weight loss. The UV-vis absorption spectra were recorded on a Perkin-Elmer Lambda 35 UV/Vis spectrometer. Steady-state emission spectra were recorded using PerkinElmer LS 50B spectrofluorometer equipped with a xenon lamp. The PLQYs were measured on an integrating sphere (Hamamatsu Photonics C9920-2). Transient PL spectra were detected on an Edinburgh fluorescence spectrometer (FLS-980). For DMAC-aza-FBKI,

the prompt (τ_p) and delayed (τ_d) lifetimes are obtained following a bi-exponential decay fitting by considering the smaller decay time as τ_p and the larger one as τ_d. For DMAC-FBKI, there just exists one decay time (τ_p) with a mono-exponential decay fitting. Atomic force microscopy (AFM) images were obtained using a Bruker MultiMode 8 atomic force microscope in tapping mode.

2. Synthesis and Characterization
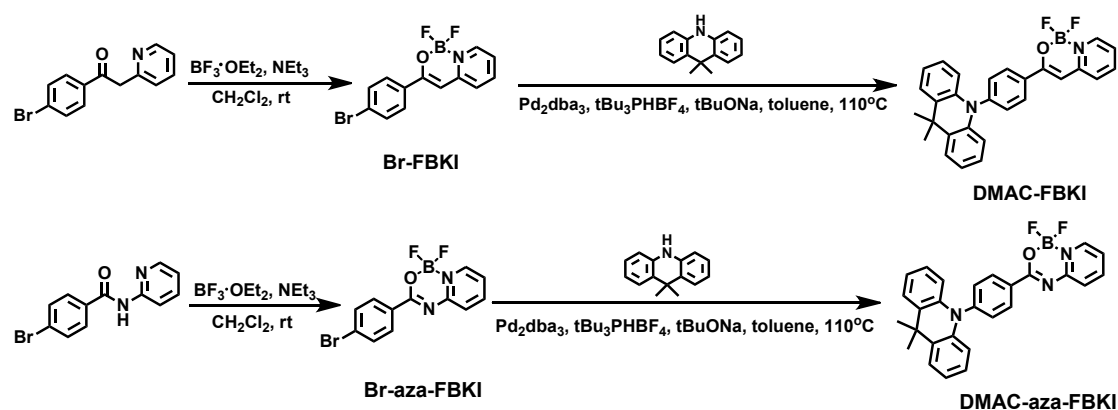
Scheme S1. Synthetic routes of DMAC-FBKI and DMAC-aza-FBKI.

FBKI, aza-FBKI, 1-(4-bromophenyl)-2-(pyridin-2-yl)ethan-1-one and 4-bromo-N-(pyridin-2-yl)benzamide were synthesized according to the previously reported method.[1-4]

Synthesis of Br-FBKI

A mixture of 1-(4-bromophenyl)-2-(pyridin-2-yl)ethan-1-one (1.9 g, 6.8 mmol), anhydrous triethylamine (13 ml, 95 mmol), and 180 mL of anhydrous dichloromethane stirred at room temperature and then boron trifluoride ethyl ether complex (20 ml, 163 mmol) was added dropwise. The reaction mixture was stirred at room temperature

overnight. Then the mixture was extracted with deionized water and dichloromethane. The organic layer was dried with anhydrous Na_2SO_4, filtered, and the filtrate was concentrated under reduced pressure. The residue was purified through column chromatography on silica gel using petroleum ether/acetyl acetate (5:1) as eluent to afford a white solid (1.4 g, 63%). ^{1}H NMR (400 MHz, $CDCl_3$) δ = 8.46 (d, J=5.5 Hz, 1H), 7.98 - 7.90 (m, 1H), 7.81 (d, J=8.6 Hz, 2H), 7.57 (d, J=8.6 Hz, 2H), 7.34 (m, 2H), 6.37 (s, 1H). ^{13}C NMR (400 MHz, $CDCl_3$) δ = 162.44, 152.20, 141.44, 140.11, 131.78, 128.01, 125.70, 122.48, 120.51, 93.61. ^{19}F NMR (400 MHz, $CDCl_3$) δ = -140.85.

Synthesis of DMAC-FBKI

A mixture of 9,9-dimethyl-9,10-dihydroacridine (DMAC, 650 mg, 3.1 mmol), Br-FBKI (1.0 g, 3.1 mmol), Pd_2dba_3 (285 mg, 0.3 mmol), t-Bu_3PHBF_4 (62.5 mg, 1.24 mmol), t-BuONa (893 mg, 9.3 mmol) and anhydrous toluene (100 ml) was added into a two-neck round bottom flask. The mixture was heated to reflux overnight under an argon atmosphere. After cooling to room temperature, the mixture was extracted with deionized water and dichloromethane, and dried over anhydrous Na_2SO_4. After removal of the solvent under reduced pressure, the crude product was purified by column chromatography on silica gel using dichloromethane/petroleum ether (1:2) as the eluent to afford a yellow solid (800 mg, 57%). ^{1}H NMR (400 MHz, $CDCl_3$) δ = 8.50 (d, J=5.8 Hz, 1H), 8.21 (d, J=8.5 Hz, 2H), 8.01 - 7.92 (m, 1H), 7.51 - 7.32 (m, 6H), 7.04 - 6.89 (m, 4H), 6.49 (s, 1H), 6.29 (dd, J=7.9, 1.3 Hz, 2H), 1.70 (s, 6H). ^{13}C NMR (400 MHz, $CDCl_3$) δ = 162.60, 151.57, 143.78, 141.49, 140.60, 140.16, 131.48, 130.18, 129.09,

126.44, 125.34, 122.55, 120.83, 120.56, 114.09, 94.87, 36.01, 31.29. ^{19}F NMR (400 MHz, CDCl$_3$) δ = -140.86. HRMS (MALDI) m/z calcd: 452.2 [M]$^+$; found: 452.3 [M]$^+$.

Synthesis of Br-aza-FBKI

This was synthesized according to a procedure similar to that for Br-FBKI. A white solid was obtained after purification by column chromatography on silica gel using petroleum ether/ethyl acetate (5:1) as eluent to afford Br-aza-FBKI in 67% yield. ^{1}H NMR (400 MHz, CDCl$_3$) δ = 8.38 (d, J=5.7 Hz, 1H), 8.25 - 8.19 (m, 2H), 8.14 - 8.08 (m, 1H), 7.66 - 7.60 (m, 2H), 7.53 (d, J=8.4 Hz, 1H), 7.44 - 7.39 (m, 1H). ^{13}C NMR (400 MHz, CDCl$_3$) δ = 164.76, 154.29, 143.91, 138.79, 131.78, 131.10, 128.50, 123.56, 120.83. ^{19}F NMR (400 MHz, CDCl$_3$) δ = -138.36.

Synthesis of DMAC-aza-FBKI

This was synthesized according to a procedure similar to that for DMAC-FBKI. A yellow solid was obtained after purification by column chromatography on silica gel using petroleum ether/ethyl acetate (5:1) as eluent to afford DMAC-aza-FBKI in 53% yield. ^{1}H NMR (400 MHz, CDCl$_3$) δ = 8.61 (d, J=8.5 Hz, 2H), 8.42 (d, J=5.7 Hz, 1H), 8.19 - 8.10 (m, 1H), 7.60 (d, J=8.4 Hz, 1H), 7.51-7.42 (m, 5H), 7.05 - 6.92 (m, 4H), 6.37 - 6.28 (m, 2H), 1.69 (s, 6H). ^{13}C NMR (400 MHz, CDCl$_3$) δ = 165.19, 154.47, 146.63, 143.94, 140.45, 138.84, 132.29, 131.78, 130.76, 126.45, 125.34, 123.55, 121.13, 120.85, 114.53, 36.12, 31.11. ^{19}F NMR (400 MHz, CDCl$_3$) δ = -138.46. HRMS (MALDI) m/z calcd: 453.2 [M]$^+$; found: 453.2 [M]$^+$.

3. Thermogravimetric Analysis
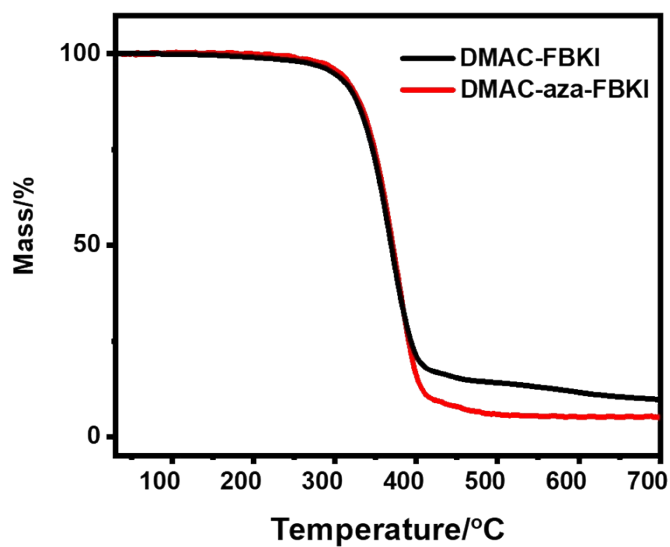

Fig. S1. TGA curves of DMAC-FBKI and DMAC-aza-FBKI.

Table S1. Thermal properties for DMAC-FBKI and DMAC-aza-FBKI.

Compounds	T_d (ºC) [a]
DMAC-FBKI	298
DMAC-aza-FBKI	306

[a] T_d were determined at 5% weight loss.

4. Photophysical properties

The photophysical properties of FBKI and aza-FBKI in toluene solutions (1×10^{-5} M) have also been investigated **(Fig. S2).** The absorption bands of FBKI and aza-FBKI are similar in shape, but the peaks of aza-FBKI are blue-shifted compared to those of FBKI. From the absorption onset, the optical band gaps (E_g^{opt}) are calculated to be 3.43 eV for aza-FBKI and 3.03 eV for FBKI, suggesting that aza-FBKI has a larger HOMO-LUMO gap. The phosphorescence (77K) bands of aza-FBKI are found to be blue-shifted compared to those of FBKI. Based on the onsets of the phosphorescence spectra, the T_1 energy levels for aza-FBKI and FBKI are determined to be 2.86 and 2.35 eV, respectively.
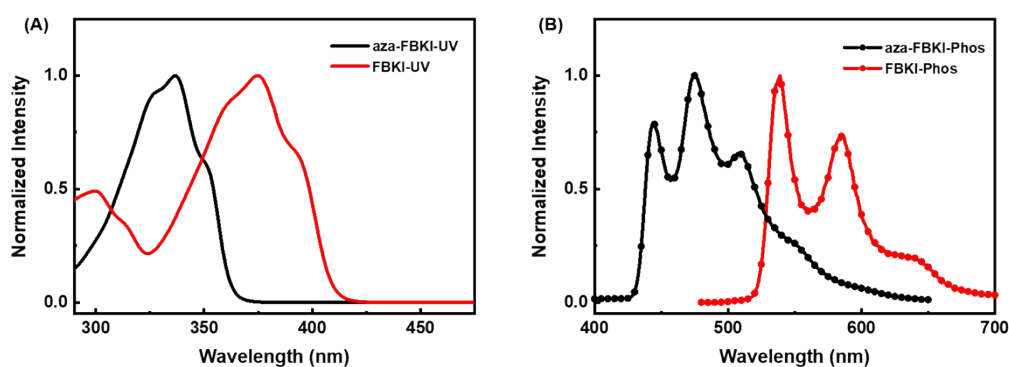
Fig. S2. Absorption (rt) (A) and phosphorescence spectra (77 K) (B) of aza-FBKI and FBKI in toluene solution (1×10^{-5} M).

Table S3. Photophysical Properties of the Difluoroboron Compounds.

Compounds	Φ_F/Φ_{DF} (%) [a]	k_r (×10⁷ s⁻¹) [b]	k_{nr} (×10⁷ s⁻¹) [b]	k_{ISC} (×10⁷ s⁻¹) [b]	k_{RISC} (×10⁶ s⁻¹) [b]
DMAC-FBKI	44/--	5.5	7.0	--	--
DMAC-aza-FBKI	25/57	1.1	0.2	3.0	1.5

[a]The PLQYs of the prompt fluorescence (Φ_{PF}) and delay fluorescence (Φ_{DF}) were calculated from the PLQYs and transient PL decay characteristic measured in doped mCP (8 wt%) film at room temperature.

[b]The rate constants of radiative (k_r) and nonradiative (k_{nr}) decay, intersystem crossing (k_{ISC}) and reverse intersystem crossing (k_{RISC}) were calculated using the following formula:[5]

$$k_r = \frac{\phi_F}{\tau_p} \tag{S1}$$

$$k_{nr} = \frac{k_r}{\phi} - k_r \tag{S2}$$

$$k_{ISC} = \frac{k_r}{\phi_F} - k_r - k_{nr} \tag{S3}$$

$$\phi_{ISC} = \frac{k_{ISC}}{k_r + k_{nr} + k_{ISC}} \tag{S4}$$

$$k_{TADF} = \frac{\phi_{DF}}{\phi_{ISC}\tau_d} \tag{S5}$$

$$k_{RISC} = \frac{k_r k_{TADF} \phi_{DF}}{k_{ISC} \phi_F} \tag{S6}$$

5. Electrochemical Studies

The HOMO and LUMO energy levels were investigated through the cyclic voltametric (CV) properties. Cyclic voltametric (CV) measurements were carried out by using a CHI660a electrochemical analyzer with 0.1 mol/L $[(n\text{-}Bu)_4N]ClO_4$ as supporting electrolyte in dichloromethane (DCM) solution at room temperature. The ferrocenium/ferrocene was used as the internal reference. $Ag/AgNO_3$ electrode, glassy carbon electrode and platinum wire were used as the reference, working and counter electrode, respectively.
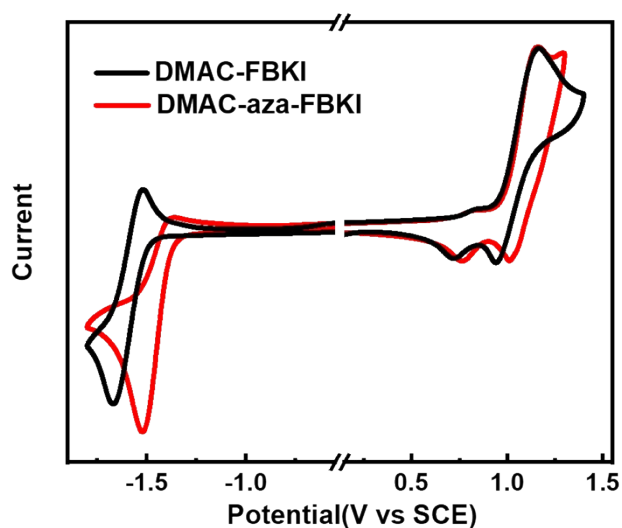
Fig. S3. CV curves of DMAC-FBKI and DMAC-aza-FBKI in CH_2Cl_2 solution.

6. Computational Details

All the density functional theory (DFT) and time-dependent DFT (TD-DFT) calculations were performed with the Gaussian 09 program suite. The ground-state (S_0) geometries of FBKI, aza-FBKI, DMAC-FBKI and DMAC-aza-FBKI were optimized by B3LYP/6-31G* level. Based on the optimized S_0 structures, TD-DFT calculations at BMK/6-31G* level were carried out to investigate the excited state properties of the four compounds. We also performed Natural Transition Orbital (NTO) analysis to estimate the characterization of the excited states as local excited (LE) and charge transfer (CT).
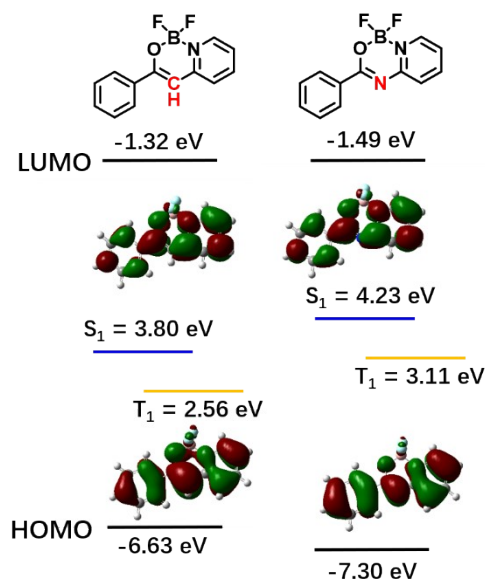
Fig. S4. HOMO and LUMO distributions based on ground state (S_0) at the B3LYP/6-31G* level for FBKI and aza-FBKI; the excitation energies of singlet (S_1) and triplet (T_1) were evaluated by TD-DFT/BMK/6-31G* level based on the optimized S_0 geometry.
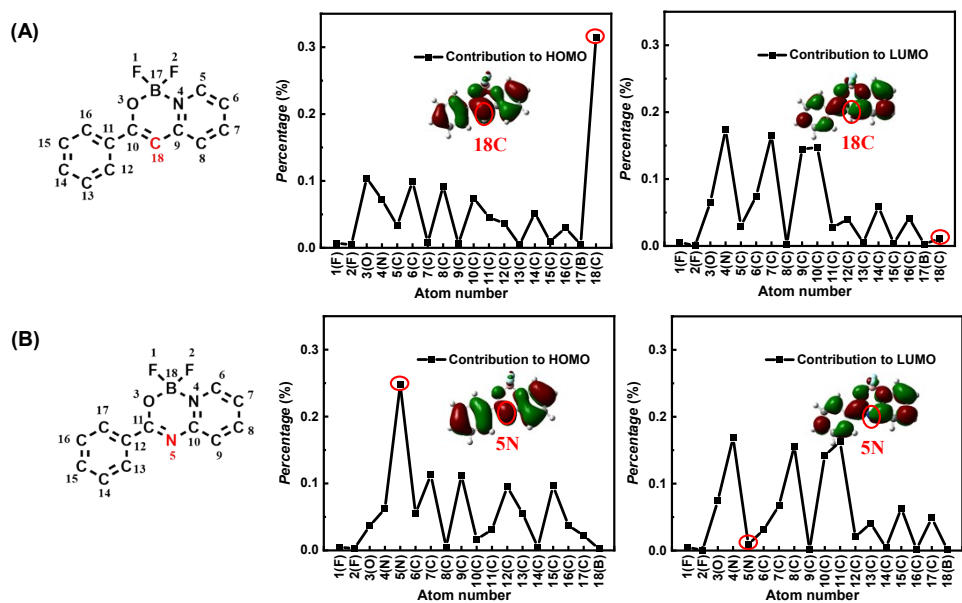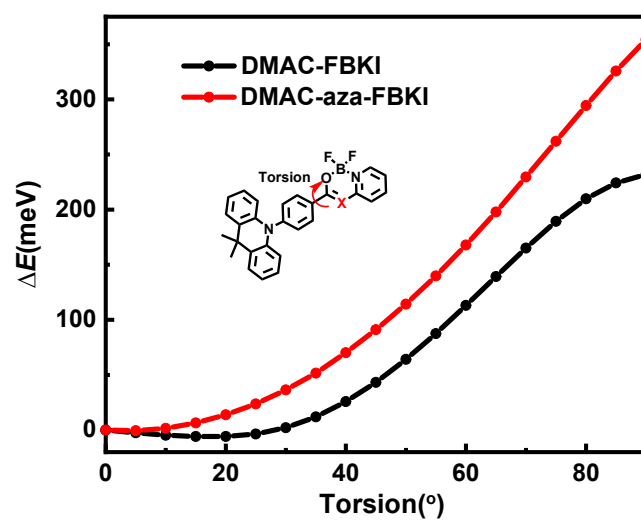
Fig. S5. Contribution of the atoms to HOMOs and LUMOs for FBKI (A) and aza-FBKI (B) by Hirshfeld method performed on Multiwfn software package (version 3.7).[6]
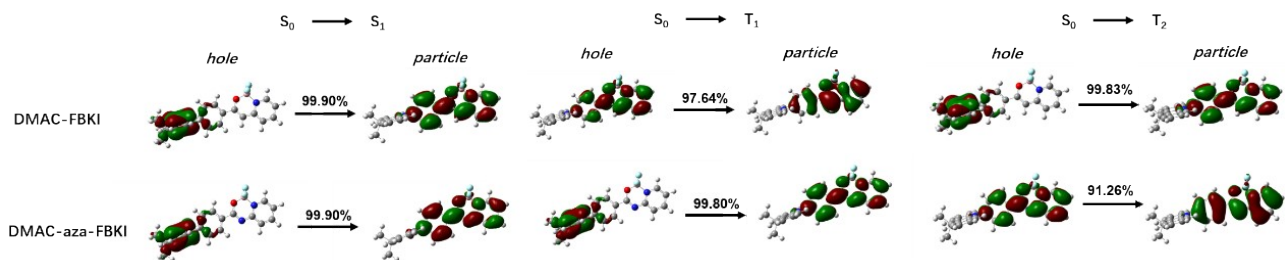
Fig. S6. NTO analysis for S_1, T_1 and T_2 of DMAC-FBKI and DMAC-aza-FBKI.
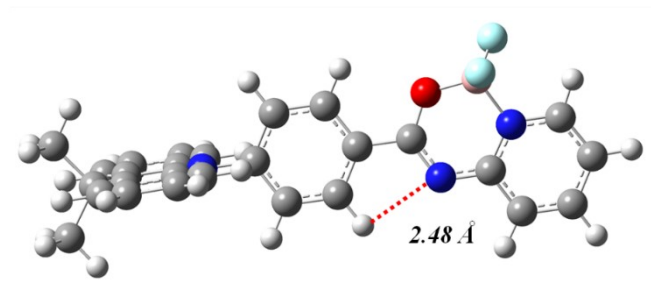
Fig. S7. The optimized molecule structures and the distance measured by GaussView 5.0 of DMAC-aza-FBKI.

**Fig. S8.** Potential energy surface for DMAC-FBKI and DMAC-aza-FBKI of the ground states in vacuum

7. OLED fabrication and characterization

7.1 Solution processed OLEDs. The device configuration is ITO/ PEDOT:PSS (30 nm)/8 wt%-emitter: mCP (40 nm)/TSPO1(8 nm)/TmPyPB (42 nm)/LiF (1 nm)/Al (100 nm). Here, ITO and Al were acted as anode and cathode, respectively. PEDOT: PSS were used as the hole injection and transporting layer. LiF and TmPyPB were utilized as the electron injection layer and electron transport layer. TSPO1 was employed as the exciton-blocking layer. mCP was selected as host because of its high T_1 energy (2.9 eV), which prevents the excited-energy of the two compounds from returning to mCP. Firstly, the ITO-coated glasses were cleaned with detergent, distilled water, then the dried substrates were treated with ultraviolet-ozone for 40 min. Subsequently, the PEDOT: PSS was spin-coated on the ITO substrates with a speed of 5000 rpm for 40 s, baked at 120 °C for 1 h, and moved into a glove box filled with N_2. Then the chlorobenzene solution of mCP and emitters were spin-coated onto PEDOT:PSS layer at a speed of 1500 rpm for 60 s to form the emissive layer. Finally, we transferred the substrates into a vacuum chamber, and the TSPO1 (8 nm), TmPyPB (42 nm), LiF (1 nm) and Al (100 nm) layers were successively vacuumed, under a pressure of about 4 $\times$ 10^{-4} Pa. Current density-voltage-luminance characteristics and electroluminescence (EL) spectra were measured using a Keithley source measurement unit (Keithley 2400 and Keithley 2000) and a CS2000 spectra colorimeter. All the devices were measured under ambient atmosphere. EQE were calculated on the basis of the EL spectrum, luminance and current density assuming a Lambertian emission distribution.

The theoretical maximum EQE can be expressed using the following equation:

$$EQE = \eta_{int} \times \eta_{out} = \gamma \times \eta_s \times \eta_{PL} \times \eta_{out} \qquad (S7)$$

The η_{int} is the internal quantum efficiency, η_{out} is the light out-coupling efficiency which is often assumed to be 25%. γ is the ratio of the recombined carriers of the injected carriers, $\gamma \approx 1$ for the balanced carrier recombination. η_s is the ratio of exciton utilization and the η_{PL} is the Φ_{PL} of both emitters doped in mCP with 8 wt%.
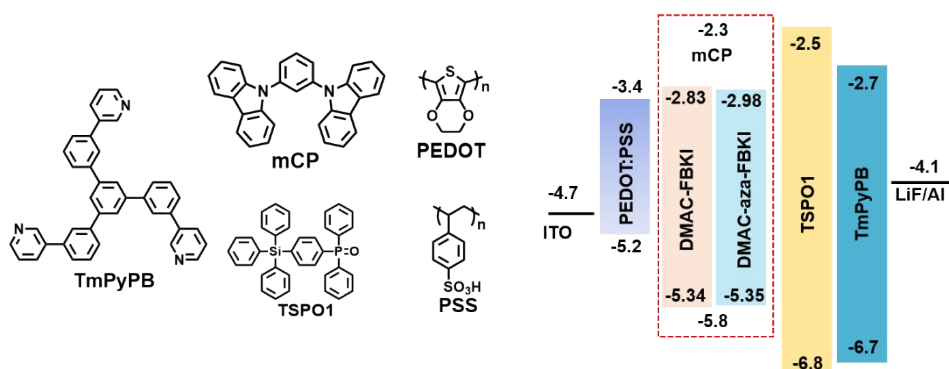
Fig. S9. Molecular structures of TmPyPB, mCP, TSPO1, PEDOT and PSS and their energy-level diagram.

7.2 Vacuum deposited OLEDs. Devices with the configuration of indium tin oxide (ITO)/ TAPC (90 nm)/ TCTA (5 nm)/ 10 wt%-emitter: mCP (30 nm)/ TSPO1(8 nm)/ TmPyPB (45 nm)/ LiF (1 nm)/ Al (150 nm) were fabricated, in which the emissive layer was prepared by co-evaporating DMAC-FBKI/mCP or DMAC-aza-FBKI/mCP at a desired concentration simultaneously (Fig. S11). The characteristics of OLEDs made with DMAC-FBKI and DMAC-aza-FBKI are shown in Fig. S10 and the corresponding data are summarized in Table S4.

Table S4. Key parameters of the vacuum deposited devices made with DMAC-aza-FBKI and DMAC-FBKI

Device	Maximum values				Values at 1000 cd m^{-2}				V_{on} (V)	EL_{max} (nm)	CIE (x, y)
	CE (cd/A)	PE (lm/W)	EQE (%)	Luminance (cd/m^2)	CE (cd/A)	PE (lm/W)	EQE (%)	Roll-off ratio (%)			
DMAC-aza-FBKI	37.6	32.0	12.3	36402	31.5	14.5	10.2	17.1	3.6	528	(0.34, 0.56)
DMAC-FBKI	7.1	5.1	2.8	8683	3.0	0.9	1.1	60.7	4.1	493	(0.22, 0.43)
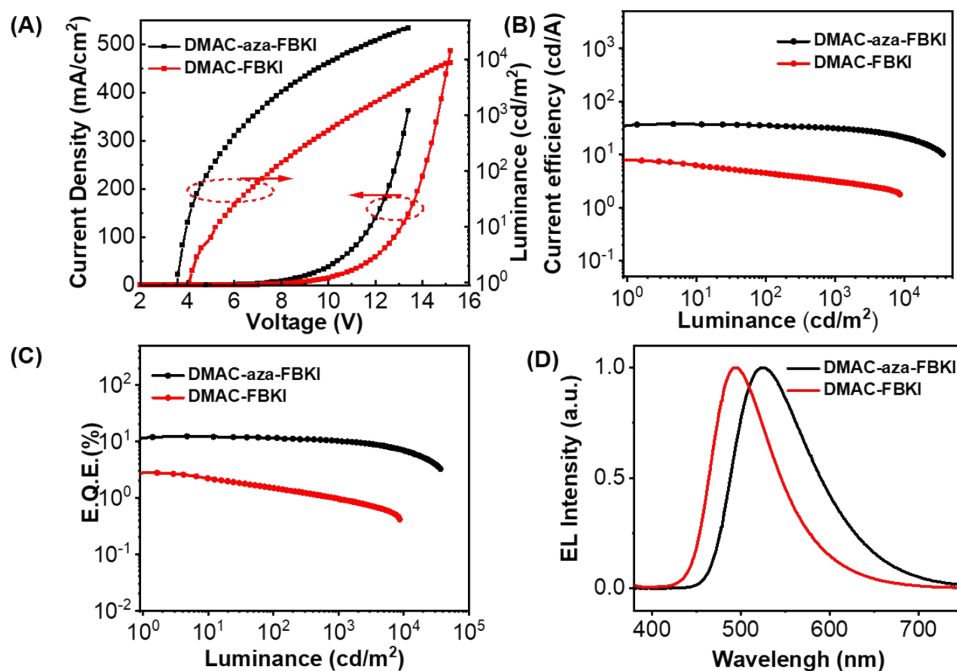
Fig. S10. Vacuum deposited devices made with DMAC-aza-FBKI and DMAC-FBKI (A) Current density–voltage–luminance (J–V–L) characteristics. (B) CE-luminance characteristics; (C) EQE as a function of Luminance; (D) Electroluminescent spectra.
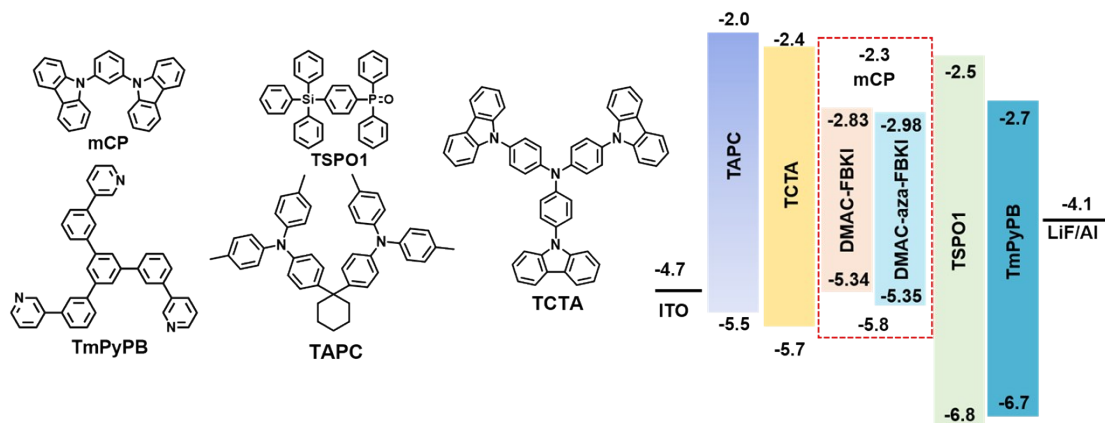

Fig. S11. Molecular structures of TmPyPB, TSPO1, mCP, TCTA and TAPC and their energy-level diagram.

8. Surface morphologies of the solution processed emissive layers

The fabrication processes of the emissive layers are the same as their solution processed OLED devices. The DMAC-FBKI and DMAC-aza-FBKI films showed a smooth surface with a root-mean-square (RMS) roughness of 0.31 nm and 0.26 nm respectively, and no obvious aggregation and phase separation were observed. [7-8]
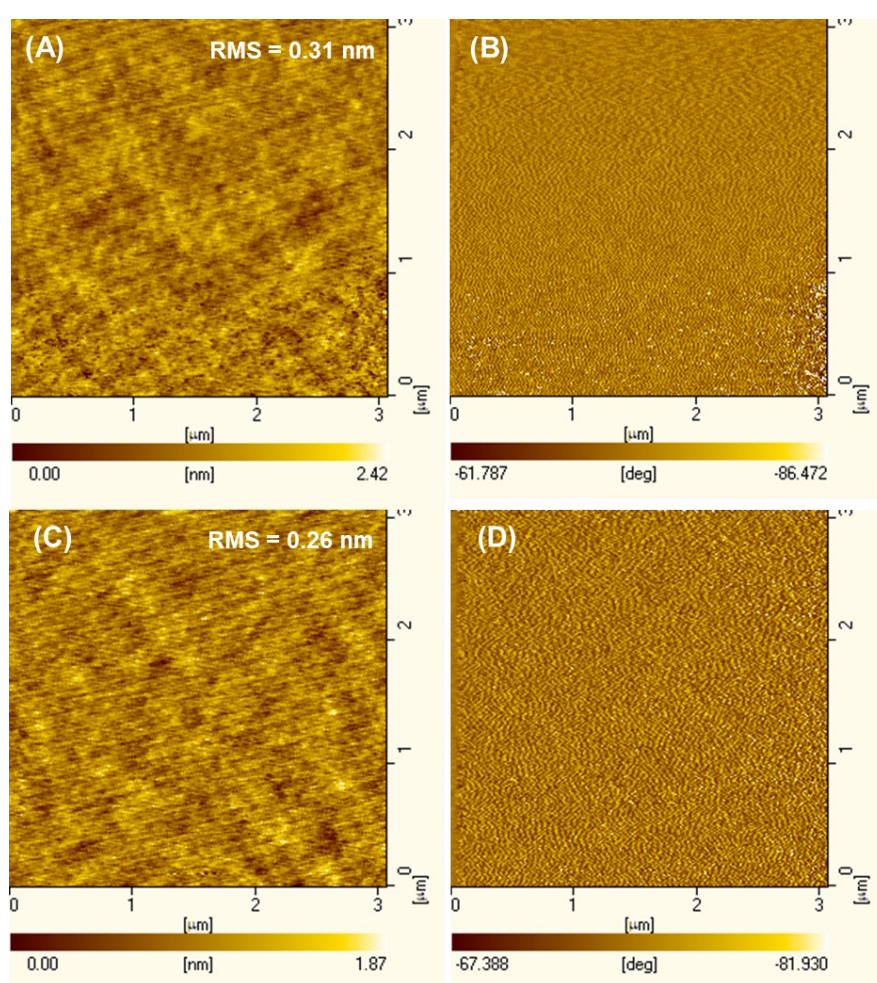
Fig. S12. AFM height and phase images of the emissive layers of DMAC-FBKI (A, B) and DMAC-aza-FBKI (C, D).

9. NMR spectra
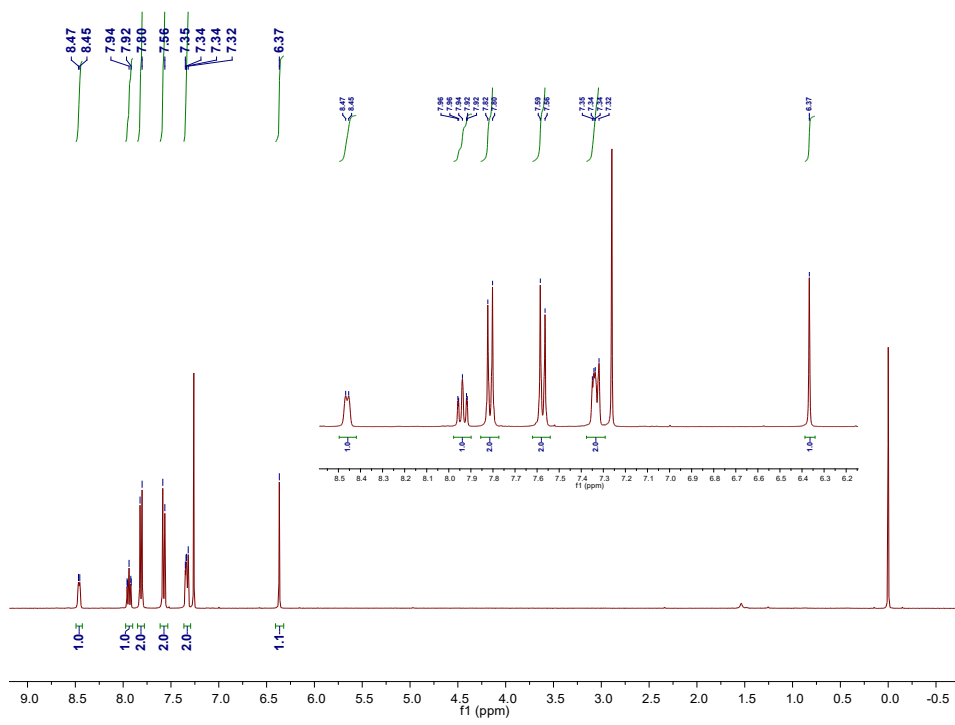
Fig. S13. ¹H NMR of Br-FBKI.
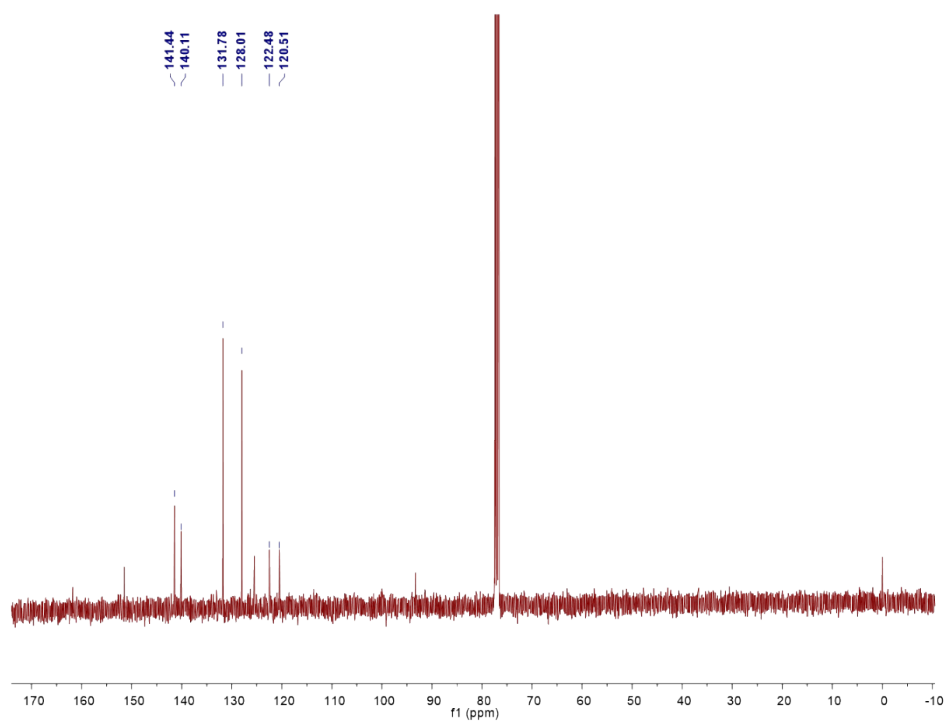
Fig. S14. ¹³C NMR of Br-FBKI.

-140.79
-140.83
-140.87
-140.91
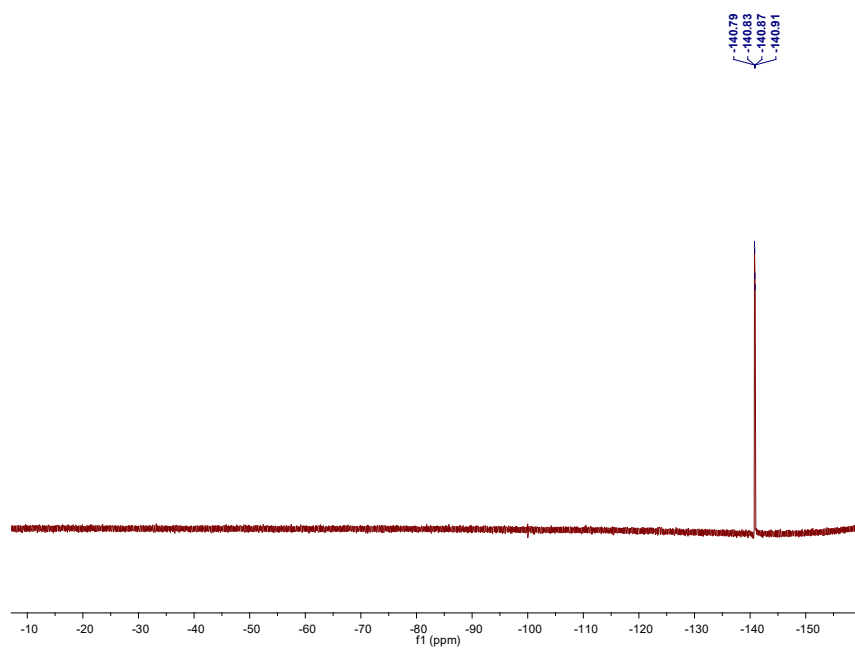
Fig. S15. ^{19}F NMR of Br-FBKI.
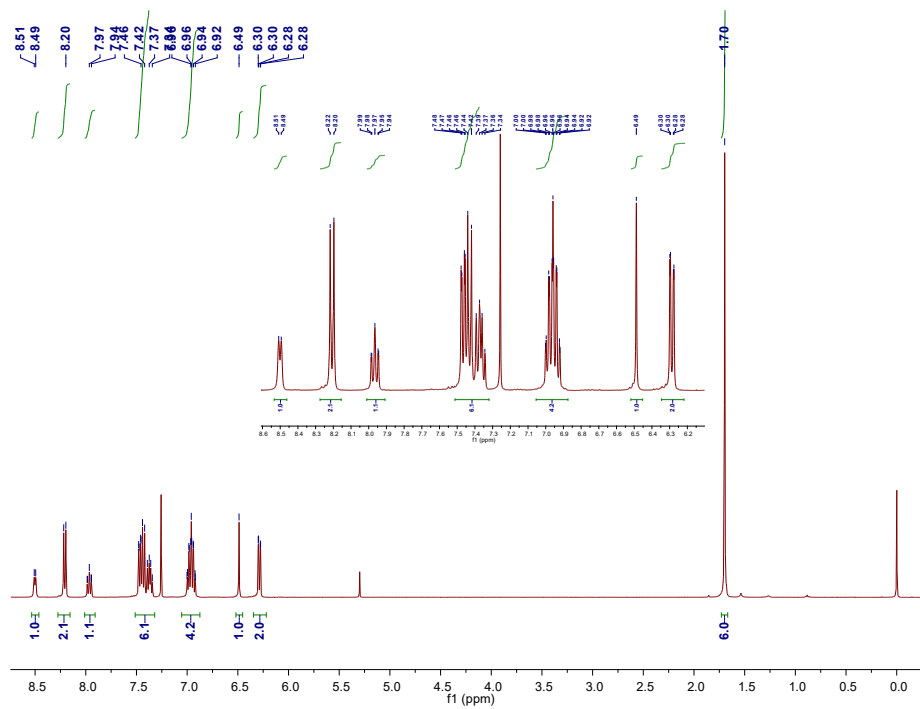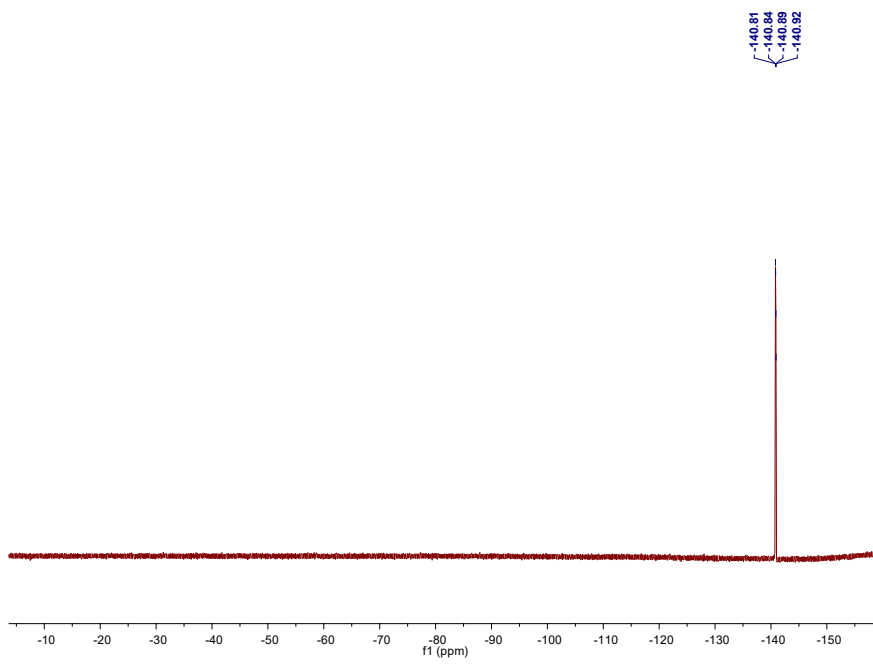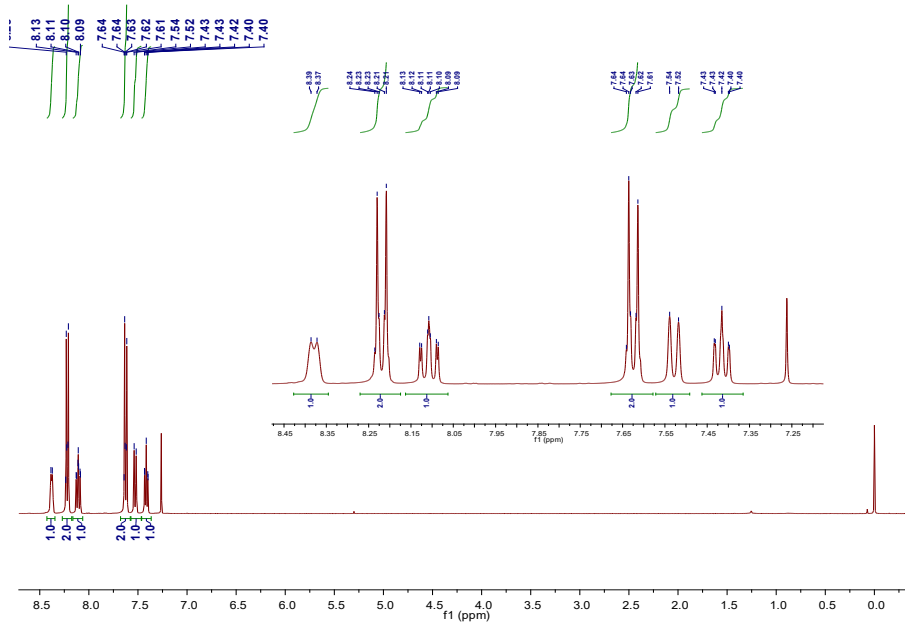
Fig.
S16.

¹H NMR of DMAC-FBKI.
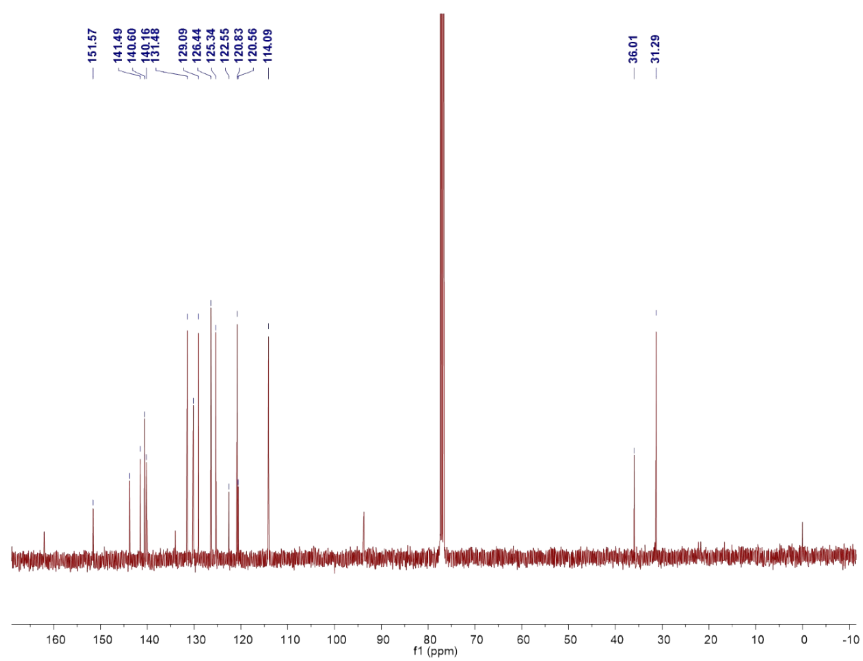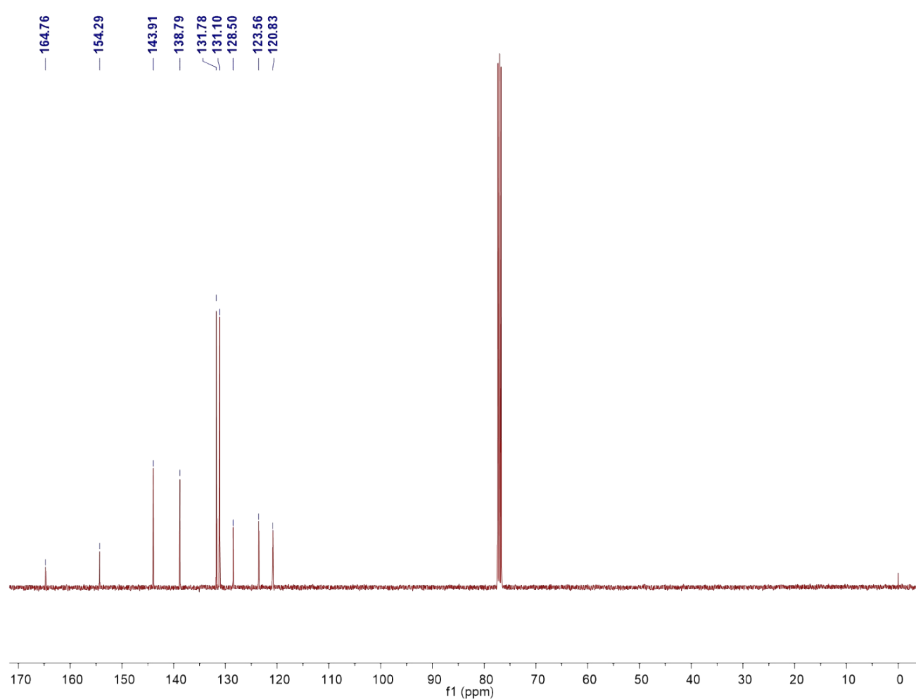

Fig. S17. ¹³C NMR of DMAC-FBKI.

Fig. S18. ^{19}F NMR of DMAC-FBKI.

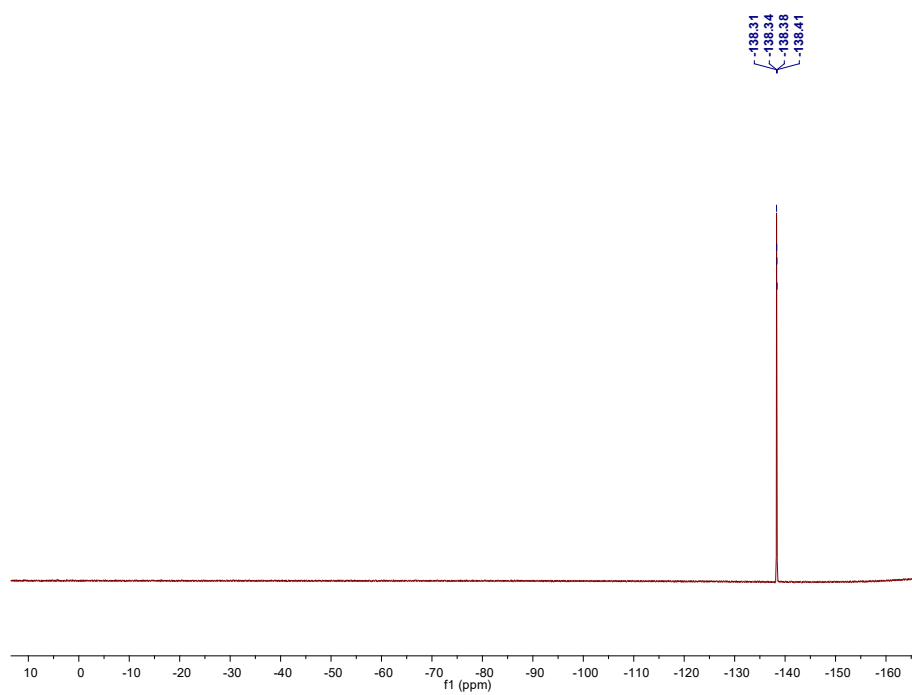**Fig. S19.**

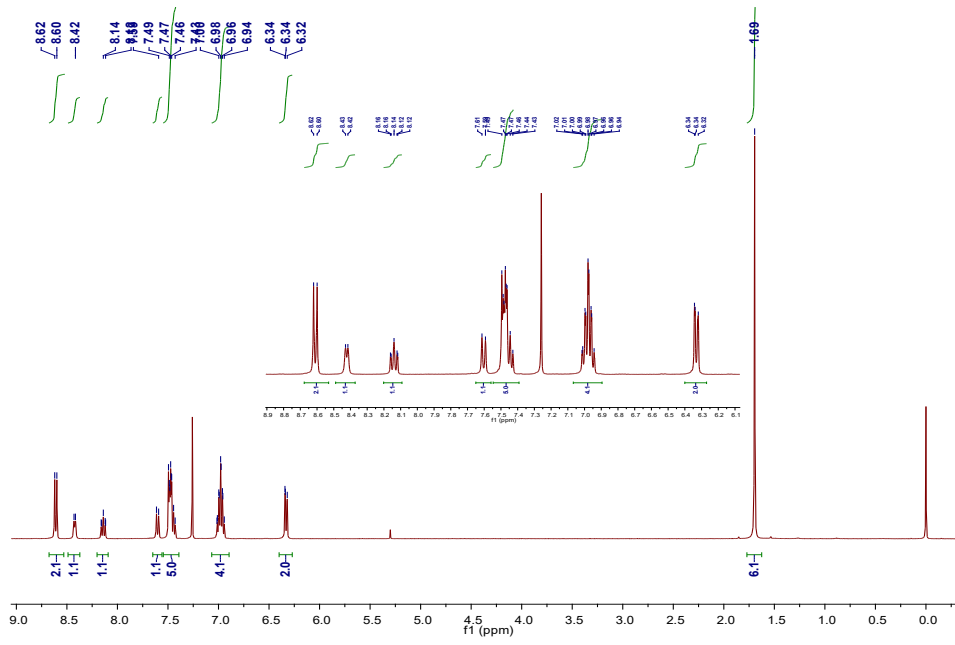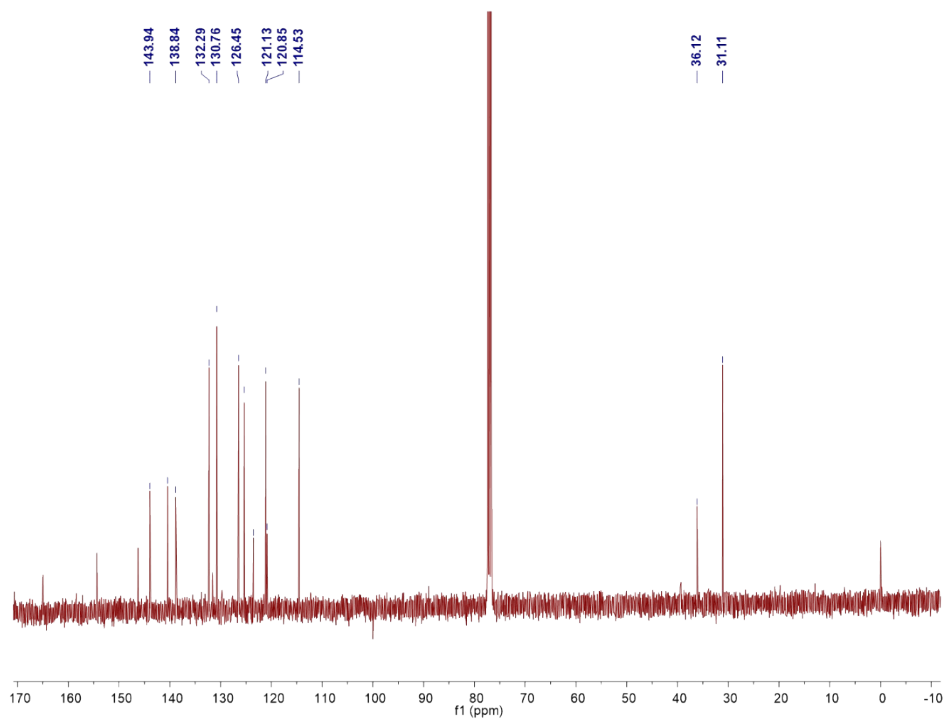¹H NMR of Br-aza-FBKI.

Fig. S20. ¹³C NMR of Br-aza-FBKI.
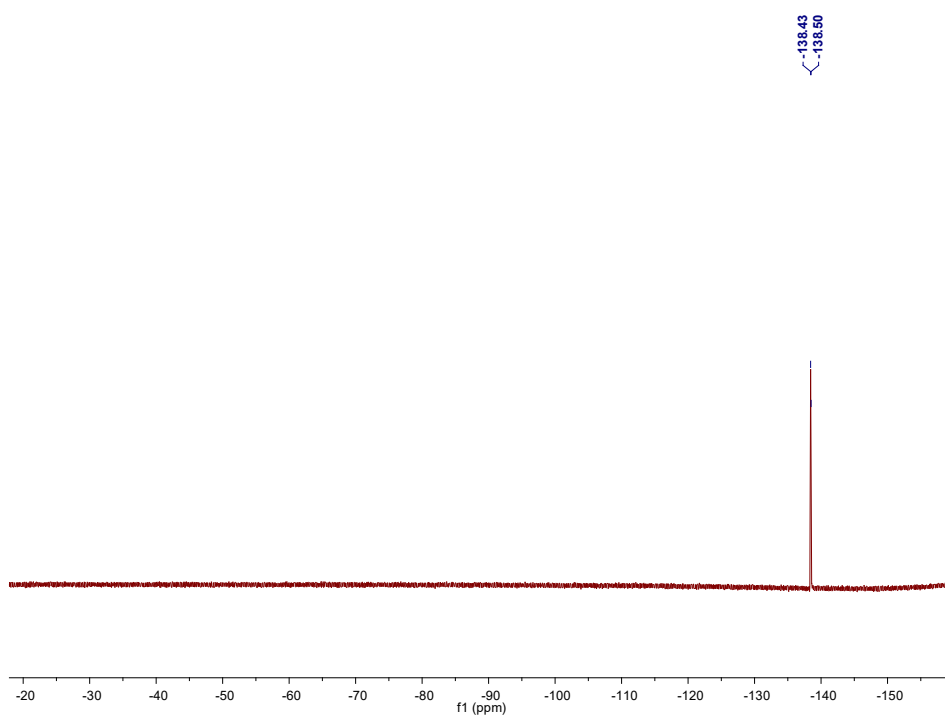
Fig. S21. ^{19}F NMR of Br-aza-FBKI.

Fig. S22. ^{1}H NMR of DMAC-aza-FBKI.

Fig. S23. ^{13}C NMR of DMAC-aza-FBKI.

Fig. S24. ^{19}F NMR of DMAC-aza-FBKI.

9. References

1   C. W. Muir, A. R. Kennedy, J. M. Redmond, A. J. B. Watson, *Org. Biomol. Chem.* 2013, **11**, 3337-3340.

2   S. Saotome, K. Suenaga, K. Tanaka, Y. Chujo, *Mater. Chem. Front.* 2020, **4,** 1781-1788.

3   M. Yamaji, S. I. Kato, K. Tomonari, M. Mamiya, K. Goto, H. Okamoto, Y. Nakamura, F. Tani, *Inorg. Chem.* 2017, **56**, 12514-12519.

4   S. Z. Yang, H. Yan, X. Y. Ren, X. K. Shi, J. Li, Y. L. Wang, G. S. Huang, *Tetrahedron.* 2013, **69**, 6431-6435.

5   T. L. Wu, S. H. Lo, Y. C. Chang, M. J. Huang, C. H. Cheng, *ACS Appl. Mater. Interfaces.* 2019, **11**, 10768-10776.

6   T. Lu, F. Chen, *J. Comput. Chem.* 2012, **33**, 580-592.

7   Y. W. Liu, X. F. Wei, Z. Y. Li, J. J. Liu, R. F. Wang, X. X. Hu, P. F. Wang, T. Qi, Y. Wang, *Adv. Opt. Mater.* 2018, **6**, 1800978.

8   P. Therdkatanyuphong, C. Kaiyasuan, P. Chasing, T. Kaewpuang, T. Chawanpunyawat, P. Wongkaew, T. Sudyoadsuk, V. Promarak, *Mater. Chem. Front.* 2020, **4**, 2943-2953.